A multiband flexible terahertz metamaterial with curvature sensing functionality

2016 J. Opt. 18 075101

(http://iopscience.iop.org/2040-8986/18/7/075101)

IOP Publishing Journal of Optics
J. Opt. 18 (2016) 075101 (7pp) doi:10.1088/2040-8978/18/7/075101

A multiband flexible terahertz metamaterial with curvature sensing functionality

Xiaoqing Zhao[1], Bin Yang[1], Jingquan Liu[1], Prakash Pitchappa[2], Dihan Hasan[2], Chong Pei Ho[2], Chunsheng Yang[1] and Chengkuo Lee[2]

[1] National Key Laboratory of Science and Technology on Micro/Nano Fabrication, Department of Micro/Nano Electronics, Shanghai Jiao Tong University, Dong Chuan Road 800, 200240 Shanghai, People's Republic of China
[2] Department of Electrical and Computer Engineering, National University of Singapore, 4 Engineering Drive 3, Singapore 117576

E-mail: binyang@sjtu.edu.cn

Received 29 February 2016, revised 20 April 2016
Accepted for publication 29 April 2016
Published 18 May 2016

Abstract
In this paper, we present a multiband flexible metamaterial in which one resonance acts as a strain sensor, while the others remain unchanged with bending strain, which might occur due to wrapping around an irregular curved surface. From both experiment and simulation, four transmission dips were observed at around 0.51, 1.34, 1.72 and 1.81 THz, respectively. The results indicated that the resonance dips in the flexible metamaterial arose from the different orders of dipole resonance mode. In the experiment, the frequency shift and amplitude modulation of the transmission at the first resonance increased linearly with the increase of the relative length change $\Delta l/L$ and changed as an exponential function of the applied bending strain. In addition, the first resonance frequency of the horizontal dipole blue shifted by 6.4 GHz, or about 1.29%, while the relative intensity change of 31.95% in the transmission was achieved when the strain was 2.79‰. This study promises applications in curvature sensing and other controllable metamaterial-based devices.

Keywords: multiband, flexible, terahertz metamaterials, curvature sensing

(Some figures may appear in colour only in the online journal)

1. Introduction

Terahertz (THz) metamaterials (MMs) [1–3] have attracted much research interest in the past decade because of their unique electromagnetic properties, such as a negative refractive index [4], cloaking [5], perfect focusing [6], phase discontinuities [7] and polarization manipulation [8–10]. In recent years, the fabrication and characterization of MMs designed for THz frequencies have proceeded very rapidly, and this field has attracted much attention because of potential applications in security [11], biology [12, 13] and chemistry [14]. Thus far, there have been several studies on flexible THz metamaterials, which have generally been prepared on flexible substrates, such as polydimethylsiloxane (PDMS) [15], polyethylene terephthalate (PET) [16] and polyethylene naphthalate (PEN) [17]. This kind of thin flexible metamaterial can make metamaterials into a non-planar form, which means they have more potential designs and applications than metamaterials made on rigid substrates. Most researchers focus on researching the in-plane tensile strain of flexible THz devices. Li *et al* [18] presented metamaterials realized on elastic substrates with frequency characteristics that can be tuned by mechanical stretching. Pryce *et al* [19] demonstrated the large strain mechanical deformation of a compliant metamaterial achieving resonant frequency tuning by up to a line width and exploited the mechanical control of coupled resonators to tunably enhance the infrared absorption of a molecular vibrational mode, which could provide a new degree of freedom in molecular sensing. It was noted that the stretching strain of flexible metamaterials played important roles in their applications. However, curvature strain sensitivity might also be significant for flexible devices that are principally used for irregular geometrical boundaries. In addition, Zheng *et al* [20] fabricated and characterized two types of flexible THz metamaterials on PEN substrates in order to investigate the effects of bending strain on electric–magnetic coupling. In this work, we experimentally explore the effects of curvature strain on a flexible THz metamaterial formed by four-fold rotationally symmetric dipolar resonators. What is more, the key difference between the earlier papers on mechanically tunable metamaterial [18] and dual axis strain sensing [21] and this one is that in the previous works the adjacent resonators were strongly coupled, while here the presented metamaterials do not have strong coupling between the neighboring resonators, but also show significant changes in resonant frequency with bending strain. Hence this paper reports an advanced functional metamaterial that shows robust performance for multiband resonances, while only one of the resonances responds to the external bending strain. The reported metamaterials are important for practical application, for example in multispectral THz imaging and spectroscopy.

2. Multiband flexible metamaterial

The periodic metal pattern in the flexible metamaterial (FM) was designed with four T-shaped plates arranged 90° from each other, with this constituting the basic unit of the metamaterial referred to as the split ring resonator (SRR). The geometric parameters of the FM are depicted in figure 1(a), with arm length $L = 40\ \mu$m, split wall width $I = 72\ \mu$m and line width $W = 4\ \mu$m. The FM comprises a thin gold pattern layer, sandwiched between the PDMS substrate layer and a PDMS encapsulation layer, and the period of unit cell $P = 130\ \mu$m, as shown clearly in figure 1(b). The resonator structures were fabricated using standard microfabrication techniques that were adapted to flexible. The 40 μm-thick PDMS substrate layer was obtained via standard spin-coating processes on a silicon wafer. Then, a 10 nm-thick Cr thin film was deposited as an adhesive layer using electron beam evaporation (EBE), and this was followed by the deposition of a 200 nm-thick gold (Au) layer. The Au layer was patterned to form the resonator structures using standard photolithography and etching techniques. The fabrication process was completed by spin coating and curing a final 20 μm-thick layer of PDMS on the top of the patterned sample, to protect the gold films underneath from possible damage. The sandwiched sample was then peeled from the supporting silicon wafer. The overall dimensions of the sample are approximately 30 mm × 10 mm, as shown in figure 1(c). The structural morphologies were observed using a scanning electron microscope (SEM), as shown in figure 1(d).

The designed FM structure shown in figure 1 was simulated by finite-difference time-domain (FDTD) simulation using the commercial software CST Microwave Studio. The PDMS substrate with relative permittivity $\varepsilon_{\mathrm{pi}} = 2.75$ was modeled as a lossy dielectric medium with a loss tangent of 0.0025. The metallic layer was modeled as lossy metal gold with a frequency independent conductivity of $\sigma = 4.09 \times 10^7\ \mathrm{S\ m^{-1}}$. The THz transmission response of the planar FM sample was measured using fast and slow scan-based THz time domain spectroscopy (THz-TDS). The absolute amplitude transmittance is defined as $|t(\omega)| = |E_S(\omega)/E_R(\omega)|^2$, where $\mathrm{E_S}(\omega)$ and $\mathrm{E_R}(\omega)$ are Fourier transformed amplitudes of the THz pulse transmitted through the samples and reference (air), respectively. Because of the 90° rotational symmetry of the MM structure, the transmission response was the same for both TE and TM polarizations. Figure 2(a) shows the simulated (red curve) and measured (black curve) transmission spectra for the planar FM samples. From both experiment and simulation, four transmission dips were observed at around 0.51, 1.34, 1.72 and 1.81 THz, respectively. The discrepancy between the simulation data and the experimental data for the bandwidths of the transmission bands located at 0.51 THz and 1.34 THz arose from imperfections in the device fabrication and the experiments, dimensional variation in the fabricated devices, the thickness of the coating layer and tilt in the placement of the sample for a given polarization of incident THz waves, etc. In addition, the resonances at 1.72 THz and 1.81 THz are slightly visible in the measured data, but are too weak. This discrepancy is due to the limitations of the measurement setup, which has a finite acquisition time and relatively low resolution. Furthermore, the drop in the sensitivity of the measurement system after 1.5 THz could also be a factor. In summary, the numerical simulation and measured results show reasonable agreement and the phenomenon of multiband resonance peaks can be realized by the four-fold rotational symmetric FM.

To understand the origin of the multiband resonance absorption peaks, the electric field and surface current distributions at resonance frequencies were studied and are given in figure 2(b). The incident electromagnetic wave is normal to the surface of the FM, and the electric field is along the x-direction. The directions of the currents on the metallic layer are indicated by black arrows for better clarity. At the resonant frequency of the transmission dip located at 0.51 THz, the electric field is mainly distributed in the sidebar of the arms, giving rise to a dipole-like resonance. At a frequency of 1.34 THz, the charges are strongly concentrated at the ends of the arms in the x-direction rather than being concentrated in the edge of 'T' cantilevers in the y-direction forming three parallel currents, which are along the direction of the incident electric field. At the higher frequency resonance of 1.72 THz, there is electric field coupling among units and the surface currents of the SRR appear to be suppressed, allowing the incident wave to be transmitted with a maximum amplitude of about 74.28%. As pointed out in [22–24], the investigated resonators are capable of achieving a multiple band frequency response over a broad frequency range due to the individual contributions of each sub-element of the unit cell and the coupling effects between its individual constituents. In essence, the resonance at 1.72 THz is a coupled mode between the quadrupole mode of the center arm and the dipolar mode of the outer arm. The mismatch in the resonance frequency causes an asymmetric resonance shape in the transmission spectrum of the metamaterial. The strong electric field localization associated with the sharp transmission peak at 1.81 THz, referred to as the Fano-like resonance [25], is seen along all the arms of the SRRs. This is direct evidence

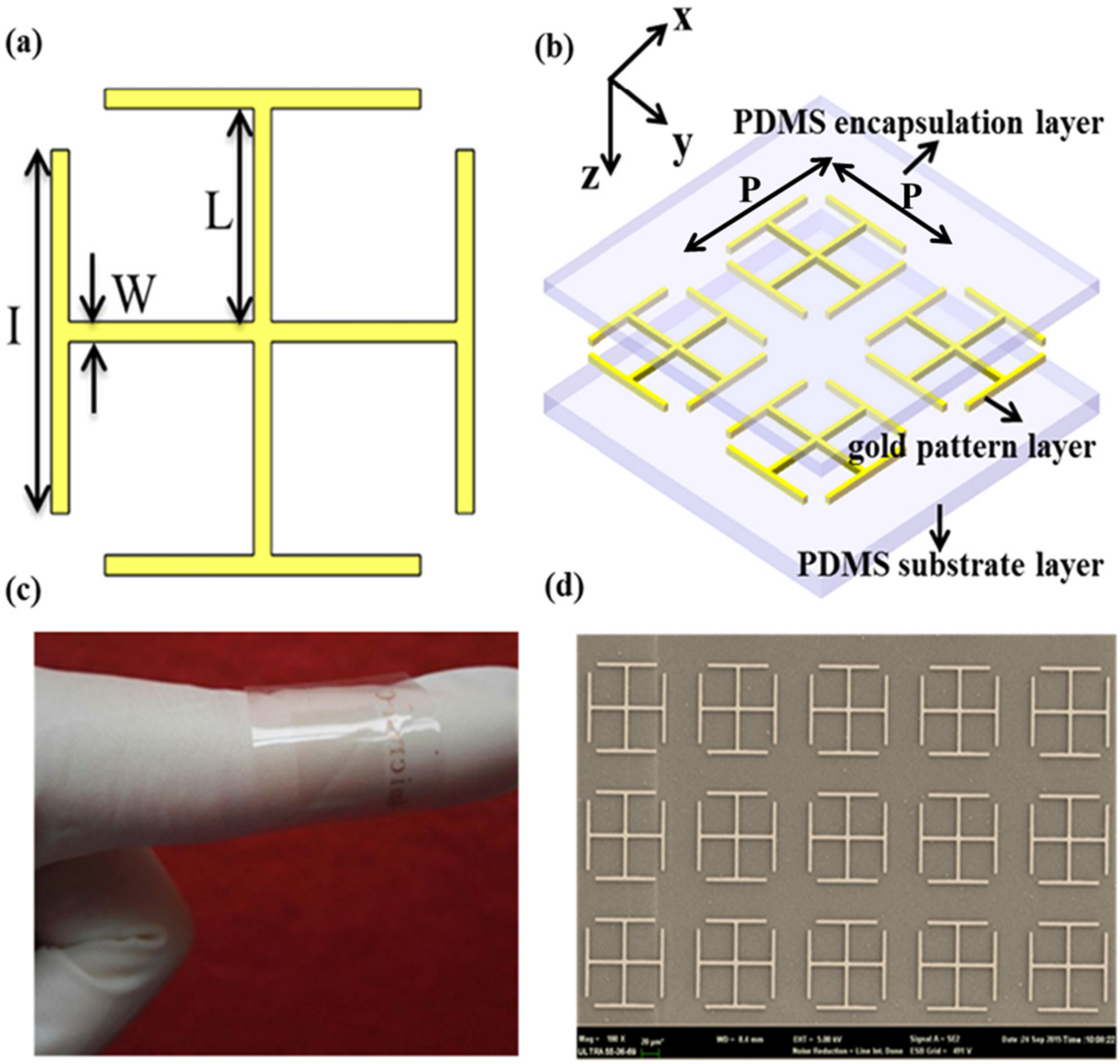

Figure 1. (a) Top view of the flexible metamaterial unit cell with $L = 40\ \mu$m, $I = 72\ \mu$m and $W = 4\ \mu$m. (b) Schematic view of the metamaterial with a sandwich structure, and the period of unit cell $P = 130\ \mu$m. (c) Photograph of the flexible metamaterial fabricated on PDMS substrate. (d) SEM image of the fabricated flexible metamaterial.

that the resonance dips in the FM arise from the dipole resonance.

3. Curvature sensing

To investigate the strain sensitivity, the fabricated metamaterial is mounted on a home-made test jig, as shown in figure 3(a), which allows easy bending of the samples with electrically moving components under a nitrogen environment. The inset of figure 3(a) shows a schematic drawing of the curved FM. The initial sample length, the distance between two fixed ends, is $L = 22.5$ mm. The bending is applied in discrete steps, with 0.5 mm defining the step size, which is equal to 2.2% strain of the initial sample length. The changes in the distance, Δl, increased from 0 to 2.5 mm, corresponding to the relative length change $\Delta l/L \times 100\%$, varied by up to 11.1%. In figure 3(b), the transmission spectrum at the first frequency assumes disciplinary changes in both the frequency and the amplitude, while those at a higher resonance frequency are not observed in measurements due to the larger noise of THz-TDS in the high frequency. As bending is applied along the horizontal direction up to 11.1%, the first resonance frequency of the horizontal dipole blue shifts upward by 6.4 GHz, or about 1.29%, as shown in figure 3(c). A wide variation in transmission amplitudes from 0.12 to 0.16 is also observed when $\Delta l/L$ is changed from zero to 11.1%. The relative intensity change in transmission $\Delta T/T \times 100\% = 31.95\%$ is achieved when the relative length change $\Delta l/L$ is 11.1%. The resonance frequency at 0.51 THz shows a blue shift with increasing bending strain due to the decreased capacitance between adjacent unit cells that are weakly coupled. However, in the case of 1.34 THz, the resonance frequency does not shift much with applied bending strain, because this mode is a dipolar mode of the outer arms (OA2 and OA4) for Ex incidence. Hence with bending

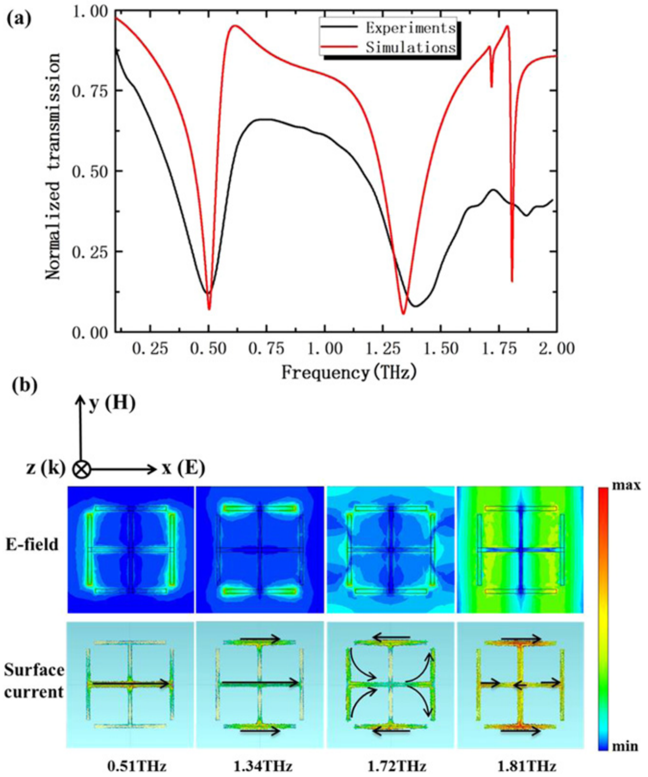

Figure 2. (a) Measured and simulated transmission spectra of planar FM. (b) The electric field and surface current distribution of FM at resonance dips of 0.51 THz, 1.34 THz, 1.72 THz and 1.81 THz.

strain, the resonance frequency shift is negligible. However, the intensity of the resonance is modulated, which primarily occurs due to the curvature of the metamaterial.

Figures 4(a) and (b) show the frequency shift (Δf) and amplitude modulation (ΔT) change as a function of the relative length change $\Delta l/L \times 100\%$, respectively, for the first resonant mode of the metamaterial. The frequency shift (Δf) and amplitude modulation of the transmission (ΔT) at the first resonance (appearing nominally at $f1 = 0.51$ THz) increase linearly with the increase of the relative length change $\Delta l/L$. Linear fitting functions are used to fit the curves and evaluate the sensitivity of the sensor. The fitting functions are described by $\Delta f = -0.641 + 0.564 \times (\Delta l/L)$, $\Delta T = 0.129 + 0.311 \times (\Delta l/L)$, which indicate the reasonably linear sensitivity level of about 0.564 GHz/% and 0.311%/% strain, respectively. As pointed out in the literature, the curvature radius R at the center of the bending FM is a function of the distance between two fixed ends $L = 22.5$ mm and the changes Δl, which can be expressed as [20]:

$$R = \frac{L}{2\pi\sqrt{\frac{\Delta l}{L} - \frac{\pi^2 W^2}{12_L{}^2}}}$$

where $W = 60\ \mu$m is the thickness of the FM. The maximum strain at the top of the bending metamaterials can be calculated as

$$\varepsilon = \frac{W}{2R}$$

which is dimensionless.

We can observe that the relationship of the frequency shift (Δf) and amplitude modulation (ΔT) change as a function of the applied bending strain (figures 4(c) and (d)) and follow exponential evolution described by

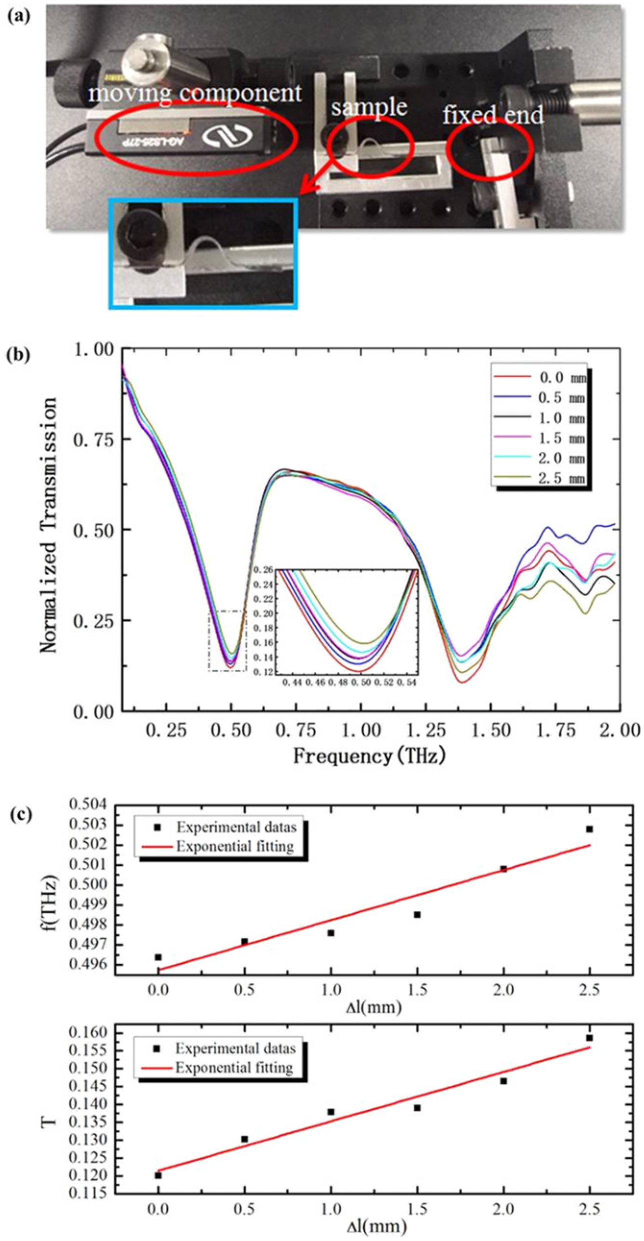

Figure 3. (a) Top views of the test jig for stretching the metamaterial with controllable strain. (b) Measured transmission spectra under the compression varying from 0 to 2.5 mm. (c) The peak frequency positions and amplitudes of the first resonance at around 0.51 THz under compression varying from 0 to 2.5 mm.

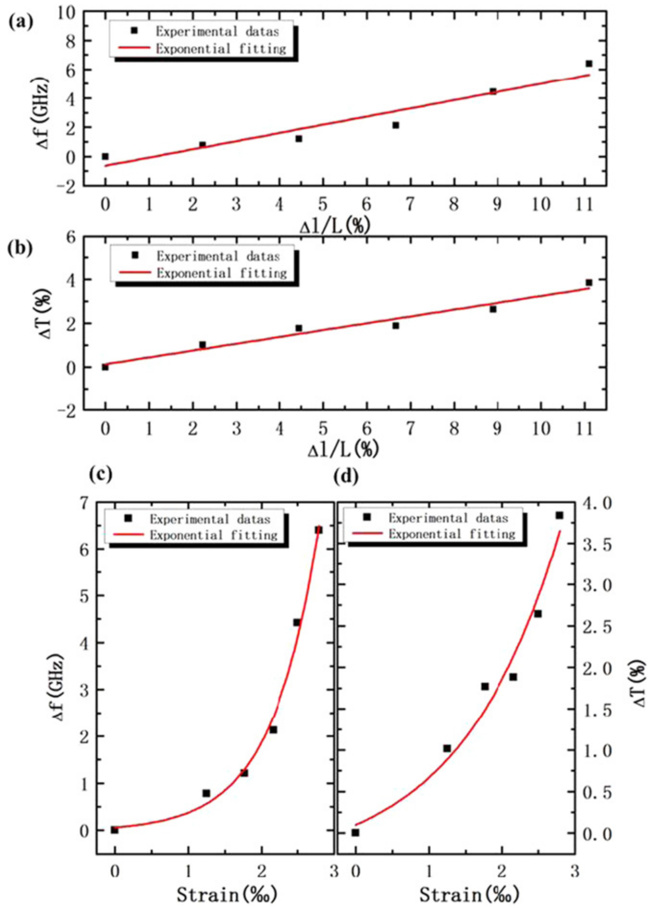

Figure 4. (a), (c) Frequency shift (Δf) and (b), (d) amplitude modulation (ΔT) versus $\Delta l/L$ and strain for the first resonant mode of the metamaterial.

$$\Delta f = -0.025 + 0.085 \times \exp(\varepsilon/0.643),$$

$$\Delta T = -0.433 + 0.532 \times \exp(\varepsilon/1.370).$$

4. Discussion

For this case, with the SRRs in plane, the electric field E in the X direction drives dipolar currents, leading to a strong decrease in the transmission at 0.51 THz. Now, however, as the sample bending reorients the SRRs out of the XY plane, the effective size of the structure decreases along the incident electric field. Hence, the resonance frequency of the FM increases as the FM bends [26]. For any bending strain of the FM, no component of H ever pierces the plane of the SRR and thus no magnetic resonance is possible. The resonant response is purely electric. Furthermore, with increased bending of the FM sample, the electric resonance strength decreases, which in turn leads to an increase in transmission. Thus, the 31.95% increase in transmission results from an electric resonance that is driven entirely by the incident electric field [27]. The numerical simulation is carried out to further study the electric interactions among the neighboring

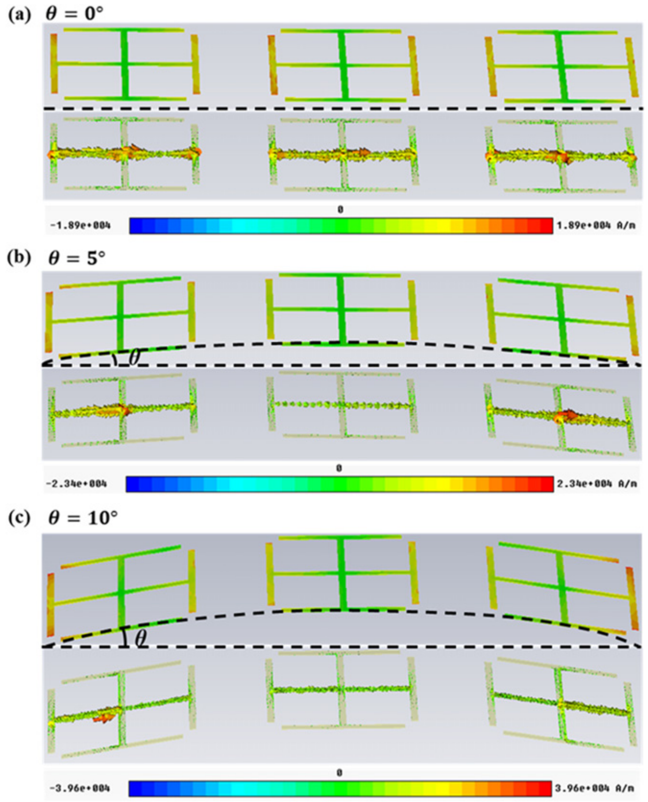

Figure 5. (a)–(c) Electric field and current density distributions of the FM at different angles among the neighboring SRRs.

SRRs. Three SRR unit cells at an angle θ are adopted in the simulation. The electric field distributions and oscillation currents at the top of the bending metamaterials are presented in figures 5(a)–(c). The electric field intensity and the oscillation current at the center become weaker as the angle θ among the neighboring SRRs increases. This is a proof of the destructive electric interactions among the neighboring SRR unit cells. In addition, when the strain leads to changes of the geometric parameters in the individual SRR, the near and far field properties of the horizontal dipole radiation and reflection phase will be affected, resulting in enhanced transmission or absorption from destructive or constructive interference between two radiative and dark modes [28–30], which might be of interest for studies on curvature sensing.

5. Summary

In this paper, electromagnetic device design and the fabrication of flexible electronics are integrated to demonstrate an optically transparent and flexible metamaterial operating at terahertz frequencies. The metamaterial comprises a planar array of metallic resonators sandwiched between a highly elastic polydimethylsiloxane substrate layer and an encapsulation layer. After investigating the electric field strength and the surface current distribution at the resonant frequencies, we concluded that the multiband absorptions are caused by different orders of dipole-type resonance mechanisms. The performance of this FM was studied experimentally under different strain conditions, and the strain sensitivity on the transmission spectra was analyzed. Utilizing the resonant elements on a highly elastomeric substrate, we achieved a continuous tunability for the first resonance frequency and amplitude modulation with a small applied strain. The first resonance of the metamaterial at 0.51 THz was responsive to deformation of the flexible substrate because of the change in the effective size of the resonator structure. Specifically, a sensitivity level of 0.564 GHz/% with a nonlinearity error of less than 11% was observed in the measurements. By adding the curvature to the resonators, a resonant frequency shift of about 1.29% and a relative intensity change in transmission of 31.95% could be obtained when the strain was $\varepsilon = 2.79‰$. Essentially, we have reported a smart metamaterial that can provide information about the curvature of the wrapped surface, while the higher order resonances remain robust. This work suggests potential applications for metamaterials in biocompatible curvature sensing.

Acknowledgments

The authors are grateful for financial support from the National Natural Science Foundation of China under grant no. 61204119, the 973 Program (2013CB329401), the Innovation Program of Shanghai Municipal Education Commission under grant no. 14ZZ019 and the Science and Technology Department of Shanghai (no. 11JC1405700).

References

[1] Han Z, Kohno K, Fujita H, Hirakawa K and Toshiyoshi H 2014 MEMS reconfigurable metamaterial for terahertz switchable filter and modulator *Opt. Express* **22** 21326–39
[2] Han Z, Kohno K, Fujita H, Hirakawa K and Toshiyoshi H 2015 Tunable terahertz filter and modulator based on electrostatic MEMS reconfigurable SRR array *IEEE J. Sel. Top. Quantum Electron.* **21** 2700809
[3] Han Z, Kohno K, Makela T, Haatainen T, Fujita H, Hirakawa K and Toshiyoshi H 2014 A MEMS reconfigurable metamaterial for terahertz filter applications *8th Int. Congress on Advanced Electromagnetic Materials in Microwaves and Optics (IEEE)* pp 346–8
[4] Valentine J, Zhang S, Zentgraf T, Ulin-Avila E, Genov D A, Bartal G and Zhang X 2008 Three-dimensional optical metamaterial with a negative refractive index *Nature* **455** 376–9
[5] Landy N and Smith D R 2012 A full-parameter unidirectional metamaterial cloak for microwaves *Nat. Mater.* **12** 25–8
[6] Fang N, Lee H, Sun C and Zhang X 2005 Sub-diffraction-limited optical imaging with a silver superlens *Science* **308** 534–7
[7] Zhang X, Tian Z, Yue W, Gu J, Zhang S, Han J and Zhang W 2013 Broadband terahertz wave deflection based on C-shape complex metamaterials with phase discontinuities *Adv. Mater.* **25** 4567–72
[8] Plum E, Zhou J, Dong J, Fedotov V A, Koschny T, Soukoulis C M and Zheludev N I 2009 Metamaterial with negative index due to chirality *Phys. Rev.* B **79** 035407
[9] Ho C P, Pitchappa P, Lin Y-S, Huang C-Y, Kropelnicki P and Lee C 2014 Electrothermally actuated microelectromechanical systems based omega-ring terahertz metamaterial with polarization dependent characteristics *Appl. Phys. Lett.* **104** 161104
[10] Pitchappa P, Ho C P, Qian Y, Dhakar L, Singh N and Lee C 2015 Microelectromechanically tunable multiband metamaterial with preserved isotropy *Sci. Rep.* **5** 11678
[11] Liu H-B, Chen Y, Bastiaans G J and Zhang X-C 2006 Detection and identification of explosive RDX by THz diffuse reflection spectroscopy *Opt. Express* **14** 415–23
[12] Globus T R, Woolard D L, Khromova T, Crowe T W, Bykhovskaia M, Gelmont B L, Hesler J and Samuels A C 2003 THz-spectroscopy of biological molecules *J. Biol. Phys.* **29** 89–100
[13] Tixier-Mita A, Segard B D, Kim Y J, Matsunaga Y, Fujita H and Toshiyoshi H 2015 TFT display panel technology as a base for biological cells electrical manipulation-application to dielectrophoresis *IEEE 28th Int. Conf. on Micro Electro Mechanical Systems (MEMS)* pp 354–7
[14] Mittleman D M, Cunningham J, Nuss M C and Geva M 1997 Noncontact semiconductor wafer characterization with the terahertz Hall effect *Appl. Phys. Lett.* **71** 16–8
[15] Ling K, Kim K and Lim S 2015 Flexible liquid metal-filled metamaterial absorber on polydimethylsiloxane (PDMS) *Opt. Express* **23** 21375–83
[16] Yoo Y J, Ju S, Park S Y, Kim Y J, Bong J, Lim T, Kim K W, Rhee J Y and Lee Y 2015 Metamaterial absorber for electromagnetic waves in periodic water droplets *Sci. Rep.* **5** 14018
[17] Han N R, Chen Z C, Lim C S, Ng B and Hong M H 2011 Broadband multi-layer terahertz metamaterials fabrication and characterization on flexible substrates *Opt. Express* **19** 6990–8
[18] Li J, Shah C M, Withayachumnankul W, Ung B S-Y, Mitchell A, Sriram S, Bhaskaran M, Chang S and Abbott D 2013 Mechanically tunable terahertz metamaterials *Appl. Phys. Lett.* **102** 121101
[19] Pryce I M, Aydin K, Kelaita Y A, Briggs R M and Atwater H A 2010 Highly strained compliant optical metamaterials with large frequency tunability *Nano Lett.* **10** 4222–7
[20] Zheng L, Sun X, Xu H, Lu Y, Lee Y, Rhee J Y and Song W 2015 Strain sensitivity of electric–magnetic coupling in flexible terahertz metamaterials *Plasmonics* **10** 1331–5
[21] Sapiens N and Agranat A J 2013 Full C-band tunable laser based on electroholography *Opt. Lett.* **38** 2131–3
[22] Yahiaoui R, Tan S, Cong L, Singh R, Yan F and Zhang W 2015 Multispectral terahertz sensing with highly flexible ultrathin metamaterial absorber *J. Appl. Phys.* **118** 083103
[23] Yahiaoui R, Guillet J P, de Miollis F and Mounaix P 2013 Ultra-flexible multiband terahertz metamaterial absorber for conformal geometry applications *Opt. Lett.* **38** 4988–90
[24] Yahiaoui R, Takano K, Miyamaru F, Hangyo M and Mounaix P 2014 Terahertz metamolecules deposited on thin flexible polymer: design, fabrication and experimental characterization *J. Opt.* **16** 094014
[25] Han S, Singh R, Cong L and Yang H 2015 Engineering the fano resonance and electromagnetically induced transparency in near-field coupled bright and dark metamaterial *J. Phys. D: Appl. Phys.* **48** 035104
[26] Ma F, Lin Y-S, Zhang X and Lee C 2014 Tunable multiband terahertz metamaterials using a reconfigurable electric split-ring resonator array *Light. Sci. Appl.* **3** e171
[27] Tao H, Strikwerda A C, Fan K, Padilla W J, Zhang X and Averitt R D 2009 Reconfigurable terahertz metamaterials *Phys. Rev. Lett.* **103** 147401

[28] Na B, Shi J, Guan C and Wang Z 2013 From electromagnetically induced transparency to absorption in planar optical metamaterials *Chin. Opt. Lett.* **11** 111602
[29] Liu T, Cao X-Y, Ma J and Wang W 2008 Effect of curvature on reflection phase characteristics of electromagnetic band-gap structures *IEEE Global Symp. on Millimeter Waves* pp 260–3
[30] Wang H-L, Fu J-H, Wu Q and Wu J 2007 Horizontal dipole radiation in the presence of a lossless metamaterial sphere *Int. Symp. on Microwave, Antenna, Propagation and EMC Technologies for Wireless Communications (2007) (IEEE)* pp 942–5